Pergamon

J. Mech. Phys. Solids, Vol. 44, No. 4, pp. 559–581, 1996

0022–5096/96 $15.00+0.00

0022–5096(95)00088–7

A GLOBAL ANALYSIS OF STRUCTURAL EVOLUTION IN A ROW OF GRAINS

B. SUN,† Z. SUO† and A. C. F. COCKS‡

†Mechanical and Environmental Engineering Department, Materials Department, University of California, Santa Barbara, CA 93106, U.S.A.; and ‡Engineering Department, Cambridge University, Cambridge CB2 1PZ, U.K.

(*Received* 27 *June* 1995; *in revised form* 28 *October* 1995)

ABSTRACT

When a polycrystalline fiber is heated for some time, grains change shape and may evolve to one of two equilibrium configurations: isolated spheres, or truncated spheres that remain connected. To which configuration do the grains evolve? How long does this evolution take? These are global questions, and call for a global way to look at the phenomenon. The fiber is a nonequilibrium structure. The free energy consists of the surface and grain-boundary energies; it is the reduction of this energy that drives the diffusive flux of atoms on the surfaces and the grain boundaries. We describe the grain shape using two generalized coordinates, the grain length and the dihedral angle. The free energy is expressed as a function of these coordinates. In the space of the free energy and the coordinates, the energy function is represented by a surface, or a landscape. A point on the landscape represents a nonequilibrium state in general, and the bottom of a valley represents an equilibrium state. We use a variational principle to assign a viscosity matrix to every point on the landscape. The approach leads to a set of ordinary differential equations that govern the evolution of the generalized coordinates.

1. INTRODUCTION

The way in which the microstructure evolves during the manufacture of a component significantly affects its performance. It is therefore necessary to understand, and be able to model, these processes at an appropriate level of sophistication. In this paper we apply a variational approach to microstructure development, which can incorporate a wide range of thermodynamic forces and mass transport mechanisms. The variational principle allows the microstructure to be described at any desired level of approximation.

We illustrate this approach by examining a problem related to some observations on a morphological change of a zirconia fiber made by Miller and Lange (1989). The fiber was drawn from a solution, placed on a sapphire plate, and heated for some time [Fig. 1(A)]. The fiber has a bamboo-like structure, with the grain boundaries perpendicular to the fiber axis. The grain diameters decrease along the fiber, but the lengths of all the grains are approximately the same. After the heat treatment, the large diameter grains remained connected [Fig. 1(B)], but the small diameter grains broke into droplets [Fig. 1(E)]. This is an example of capillary instability. The grains

change shape to reduce the total surface and grain-boundary energy, mass being transported by diffusion, creep or surface reactions. Similar phenomena involving the evolution of arrays of grains include, e.g. powder sintering (Cannon and Carter, 1989; Kellett and Lange, 1989; Sudre and Lange, 1992), and interconnect failure in integrated circuits (Srolovitz and Thompson, 1986; Klinger *et al.*, 1995).

Most models of capillarity-driven solid-state processes originate from the work of Herring (1951). For a wide range of applications, a macroscopically nonequilibrium structure may be divided into elements, each being in an equilibrium state. The free energy of an element is a function of the local state variables such as composition, temperature and stress. The total free energy of the structure is summed over all the elements. Herring defined the chemical potential of an element as the increase of the total free energy associated with the addition of one atom to the element. For the nonequilibrium structure, the chemical potential differs from one element to another. Herring assumed that the chemical potential *gradient* drives mass flux according to an empirical kinetic law. Together with mass conservation, such ideas lead to partial differential equations, quite analogous to the heat transfer problem.

An alternative, global view regards evolution as a means to release the total free energy. A nonequilibrium structure is described, often approximately, with a set of generalized coordinates. For a structure described with one degree of freedom, the free energy is a function of the generalized coordinate, represented by a curve in a plane spanned by the free energy and the coordinate. A minimum free energy point on the curve represents an equilibrium state. Thermodynamics requires that the state of the nonequilibrium structure descends on the curve toward equilibrium. Consequently, thermodynamics alone determines both the evolution path and the final state. Kinetics is restricted to the role of determining the rate of travel along the path toward the equilibrium state.

For a structure described with two degrees of freedom, the energy is a function of the two generalized coordinates. This function is pictured as a surface in a three dimensional space, with the generalized coordinate directions lying in a plane and the values of the free energy represented by a surface above this plane. A point on the surface represents a nonequilibrium state, in general, and the bottom of a valley represents an equilibrium state. Thermodynamics requires that an evolution path be a curve on the surface, descending from the initial state to the bottom of a valley. There are, however, countless descending curves on a surface. Consequently, thermodynamics by itself neither determines the evolution path, nor selects the final equilibrium state from among the available valleys.

Mistaken "laws" in this connection are sometimes proposed in scientific discussions. One such law says that a structure evolves along the trajectory of steepest descent on the energy landscape. Another such law says that a structure selects the deepest valley as its final equilibrium state. They have no scientific basis, however. It is the combination of thermodynamics *and* kinetics that determines the path and the final state. Thus, in a structure with more than one degree of freedom, kinetics plays a more significant role than just timekeeping.

Kinetics, such as atomic diffusion, proceeds locally. How can one transcribe such local information onto the landscape? A variational principle does this well: it assigns a viscosity matrix to every point on the landscape. The principle is a global version

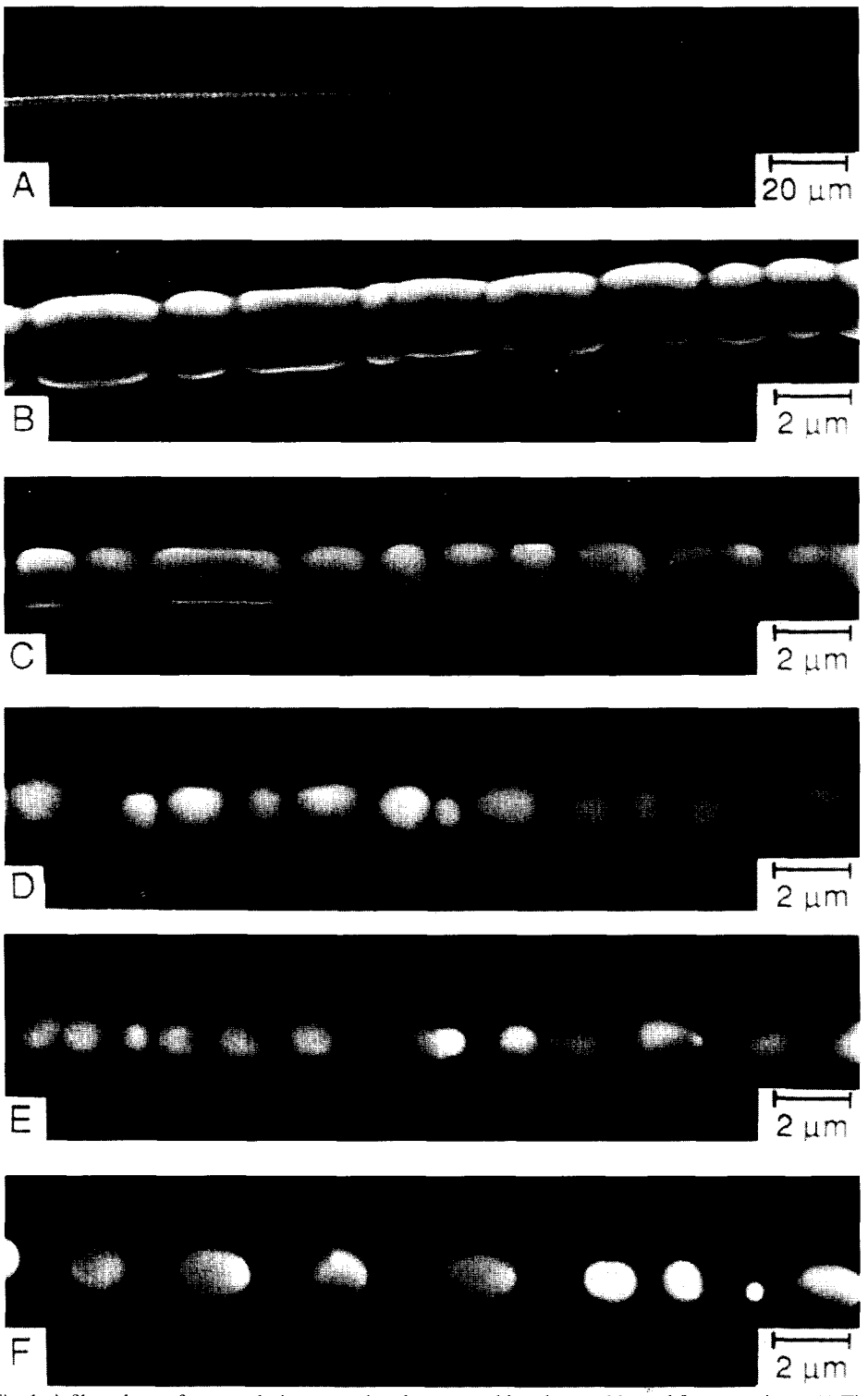

Fig. 1. A fiber, drawn from a solution, was placed on a sapphire plate and heated for some time. (A) The fiber diameter is large at one end and small at the other. (B,C) Grains with large diameters remain connected. (D,E,F) Grains with small diameters break into droplets. (Courtesy of Professor F. F. Lange.)

of Herring's nonequilibrium thermodynamics. The quantity to be minimized consists of energy rate and a term involving diffusivity.

Such variational principles have been used in modeling diverse nonequilibrium phenomena in materials. The free energy may include interfacial, elastic, electrostatic, and chemical energy. The rate process may include diffusion, creep, grain-boundary motion, and surface or interface reactions. Material phenomena include creep void growth (Needleman and Rice, 1980; Cocks and Searle, 1991; Cocks and Pan, 1994), creep crack growth (Cocks and Pan, 1993; Pan and Cocks, 1993a), superplasticity (Pan and Cocks, 1993b), interface diffusion in composites (Sofronis and McMeeking 1994), and solid-state sintering (McMeeking and Kuhn, 1992; Cocks, 1994). These authors formulated the variational principles by assembling local quantities such as chemical potentials and relating these to the boundary conditions through the principle of virtual power. Alternatively, one may formulate the variational principles from a global definition of the driving forces (Svoboda and Turek, 1991; Suo and Wang, 1994). This latter approach has been used to model phenomena including void shape instability (Sun *et al.*, 1994), dislocation climb (Suo, 1994), wrinkling of oxide scales on high temperature alloys (Suo, 1995a), ferroelectric domain evolution (Loge and Suo, 1995), grain growth (Suo, 1995b; Cocks and Gill, 1995; Gill and Cocks, 1995; Du *et al.*, 1995), solid-state sintering (Svoboda and Riedel, 1995), and electromigration-induced transgranular slits (Wang and Suo, 1995). Bower and Freund (1995) have formulated a general class of variational principles for analyzing electromigration in deformable solids.

An energy landscape only makes literal sense when the structure has two degrees of freedom. However, it offers a geometric analogy to guide the analysis in higher dimensions. Besides, many interesting phenomena can be understood by describing a structure with two degrees of freedom. The following sections will describe these ideas using the linear grain array as an example. The power and the generality of the approach will become evident as we proceed.

2. EVOLUTION DIVERSITY OF A ROW OF GRAINS

Figure 2(a) illustrates a row of identical grains, initially cylindrical in shape and connected at their ends, of length L_0 and diameter D_0. When heated, the grains change shape and are assumed to remain identical to one another [Fig. 2(b)]. In the experiment of Miller and Lange (1989), the zirconia fiber was sintered to the sapphire plate, which constrained the shrinkage of the length of the fiber. In this paper, to demonstrate several general points, we will model an experimental situation that allows the fiber length to shrink.

The surface energy γ_s and the grain-boundary energy γ_b are taken to be isotropic. At a given time, the surface of a grain has area A_s, and a grain-boundary has area A_b. The free energy per grain is

$$G = \gamma_s A_s + \gamma_b A_b. \tag{1}$$

The grains change shape to reduce the free energy. Appendix A calculates the free energy explicitly. The surfaces of two neighboring grains meet at a dihedral angle, Ψ.

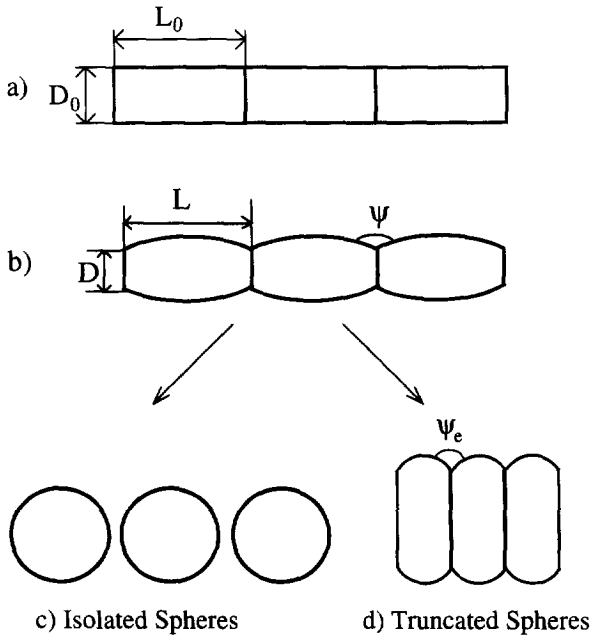

Fig. 2. (a) The initial array of cylinder-shaped grains. (b) An array of barrel-shaped grains approximate an intermediate, nonequilibrium state. (c) Grains pinch off and spheroidize, approaching an equilibrium state, a row of isolated spheres. (d) The array shrinks as atoms diffuse out from the grain boundaries and plate onto the free surfaces, approaching another equilibrium state, a touching array of truncated spheres.

In equilibrium, Ψ reaches a value, Ψ_e, determined by the surface tensions according to

$$\frac{\gamma_b}{2\gamma_s} = \cos\left(\frac{\Psi_e}{2}\right). \tag{2}$$

We will use Ψ_e to indicate the ratio of the surface and the grain-boundary tensions.

In this model two kinetic processes are allowed: atomic diffusion on the free-surfaces and on the grain boundaries. Let J_s be the atomic flux on the free-surface (i.e. the number of atoms per unit time flowing across a unit length on the surface), and F_s be the atomic driving force on the surface (i.e. the free energy reduction associated with an atom moving a unit distance on the surface). The force drives the flux according to an empirical kinetic law

$$J_s = M_s F_s. \tag{3}$$

This equation defines the atomic mobility on the free-surface, M_s. The mobility is related to the self-diffusivity by the Einstein relation, $M_s = D_s \delta_s / \Omega k T$, where D_s is the surface diffusivity, δ_s the effective thickness of surface atoms participating in mass transport, Ω the volume occupied by an atom in the interior of the solid, k Boltzmann's constant, and T the absolute temperature. One can similarly define quantities J_b, F_b and M_b for a grain boundary, and assume a kinetic law

$$J_b = M_b F_b. \tag{4}$$

Both mobilities, M_s and M_b, are taken to be independent of crystalline orientation.

In the local approach, the forces F_s and F_b are expressed in terms of local quantities such as surface curvature, surface tension, and stress (Herring, 1951). These relations are not useful in the global approach and will not be listed here. Appendix B compares the local and the global approaches.

The present model has three dimensionless *control parameters* that do not change during evolution: the initial grain aspect ratio L_0/D_0, the surface tension ratio γ_b/γ_s (or the equilibrium dihedral angle Ψ_e), and the mobility ratio M_b/M_s. The first two enter the free energy function, and the last results from the kinetic processes. We next consider qualitatively the role of each of these parameters in turn.

First consider the role of the surface tension ratio γ_b/γ_s, everything else being fixed. In an unusual situation where $\gamma_b/\gamma_s > 2$, the grains do not wet one another, and the lowest energy configuration is the isolated spheres. In a more representative situation, $\gamma_b/\gamma_s < 2$, two equilibrium configurations exist: isolated spheres [Fig. 2(c)], and truncated spheres that remain connected [Fig. 2(d)]. All subsequent discussions will be restricted to this situation. As atoms diffuse, the surface grooves along the triple junction, so that the grains may pinch off and spheroidize. Alternatively, if atoms diffuse out from every grain boundary and plate on the free surfaces, the grains shrink in length and approach a row of truncated spheres that remain connected. Of the two configurations, the isolated spheres have higher energy than the truncated spheres. This does not imply, however, that the grains always evolve into truncated spheres, as we shall see presently.

Next consider the role of the initial grain aspect ratio L_0/D_0, everything else being fixed. For a small value of L_0/D_0, the grooves are shallow compared to the grain-boundary diameter, and the grains evolve into truncated spheres. In this case, the structure does approach the lowest energy state. For a large value of L_0/D_0, the grooves break the grains; being isolated, the grains spheroidize and cannot spontaneously reconnect. In this case the structure does not select the lowest energy state: the fiber breaks before it shrinks to the truncated spheres.

Last consider the role of the mobility ratio M_b/M_s, everything else being fixed. If the grain-boundary mobility is negligible compared to the surface mobility, $M_b/M_s \ll 1$, atoms mainly diffuse along the surface and make deep grooves along the grain boundaries, causing grains to pinch off and spheroidize. If the grain-boundary mobility is appreciable, however, atoms can diffuse out from the grain boundaries and deposit on the free surfaces, allowing the grains to approach one another, resulting in truncated spheres that remain connected.

The above considerations lead us to use the control parameters as coordinates to construct a *parameter space*, in which each point represents a set of parameters. Boundaries exist to divide the space into regions. A structure with its parameter set falling in a particular region will approach a certain equilibrium state. It is often more practical to draw a map on a plane with only two control parameters as the coordinates, all other parameters being fixed. We call this a *diversity map*. Figure 3 shows such a map for $\Psi_e = 150°$, a typical value for oxides. A point on the map represents a pair of parameters, L_0/D_0 and M_b/M_s. A boundary divides the plane into two

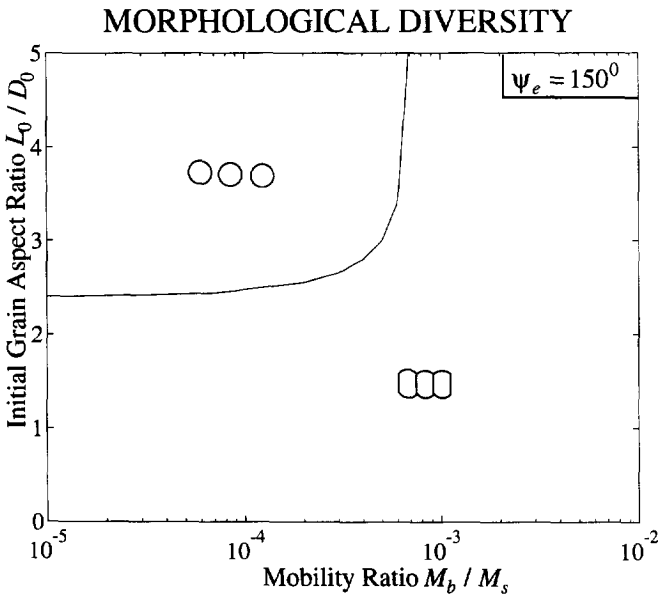

Fig. 3. A diversity map. The coordinates are the control parameters that do not change when the structure evolves. A boundary separates the plane into two regions. A fiber with the parameter group falling above the boundary evolves to isolated spheres. A fiber with the parameter group falling below the boundary evolves to truncated spheres.

regions. As indicated in Fig. 3, a parameter pair in one region makes the grains evolve to isolated spheres, and a parameter pair in the region makes the grains evolve to truncated spheres.

A diversity map contains global information of the structure. As we have already demonstrated, the existence of the boundary and the relative locations of the regions rely on general considerations. The details of the model only affect the exact position of the boundary. Given the uncertainties in the experimental data of the parameters, a simple model that yields an approximate boundary is often adequate. The boundary in Fig. 3 is determined by a model to be described in the following sections.

3. ENERGY LANDSCAPE

Miller and Lange (1989) approximated the shape of a nonequilibrium grain by a barrel formed by rotating a circular arc about a prescribed axis (Fig. 4). The geometry is fully specified by three lengths: the arc radius R, the grain length L, and the grain-boundary diameter D. The volume of each grain is taken to be conserved during evolution, which places a constraint on possible values for the three lengths. In addition, the zirconia fiber in their experiment sintered to the sapphire plate, so that grain length L remained constant before the grains pinched off. Consequently, within the approximation, a grain had only one degree of freedom, which Miller and Lange chose to be the dihedral angle, Ψ.

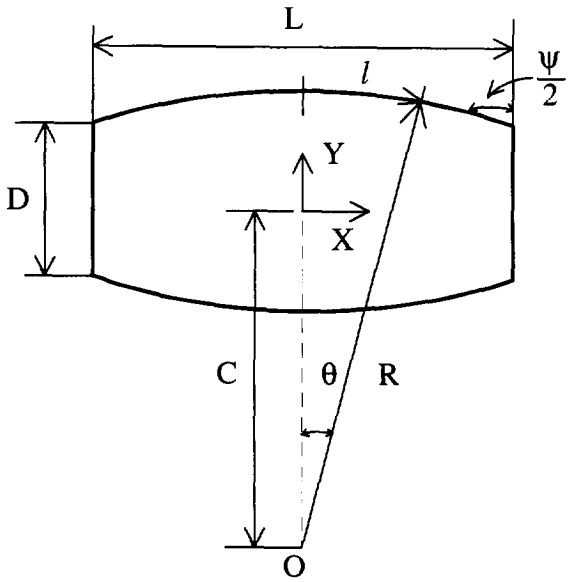

Fig. 4. Geometry of a barrel formed by revolving a circular arc. The configuration is fully determined by three lengths: the radius of the arc R, the grain length L, and the grain-boundary diameter D.

Note that the dihedral angle approaches its equilibrium value (2) instantaneously, for it only takes short range diffusion to maintain the equilibrium angle, as compared to diffusion over the grain length to maintain equilibrium of the entire grain shape. Thus, for example, Mullins (1957) required that the dihedral angle be fixed at Ψ_e during surface grooving. Such a fixation is necessary when one seeks the exact solution. However, here we seek an approximate solution. We can choose any kind of generalized coordinates, so long as they make global sense, i.e. reasonably describe the overall shape. It is unnecessary to exactly describe the shape at "selective" locations, such as triple junctions. More will be said about the dihedral angle in Section 4 and Appendix B.

The free energy, G, is the function of the generalized coordinate, Ψ. For given control parameters L_0/D_0 and γ_b/γ_s, $G(\Psi)$ is a curve in the plane of G and Ψ. An equilibrium state is a minimum on the curve, reachable if the curve descends from the initial state to the minimum. Figure 5 reproduces the results of Miller and Lange (1989), showing the energy–coordinate curve for $\Psi_e = 150°$ and several initial grain aspect ratios. The free energy, G, is normalized by the free energy of the initial cylinder-shaped grain, G_0. The dashed lines indicate the states after the grains pinch off. For a large initial aspect ratio, e.g. $L_0/D_0 = 2.5$, the energy descends from the initial state of cylinders to the state of isolated spheres, so that the grains approach this state. For a small initial aspect ratio, e.g. $L_0/D_0 = 1.5$, the energy reaches a minimum when the grains still remain connected, at a dihedral angle close to 150°. Consequently, a critical value L_0/D_0 exists, above which the fiber breaks into droplets. In Miller and Lange's experiments the fiber was tapered and the diameter of the grains decreased along the length of the fiber towards its tip, but all the grains were of a

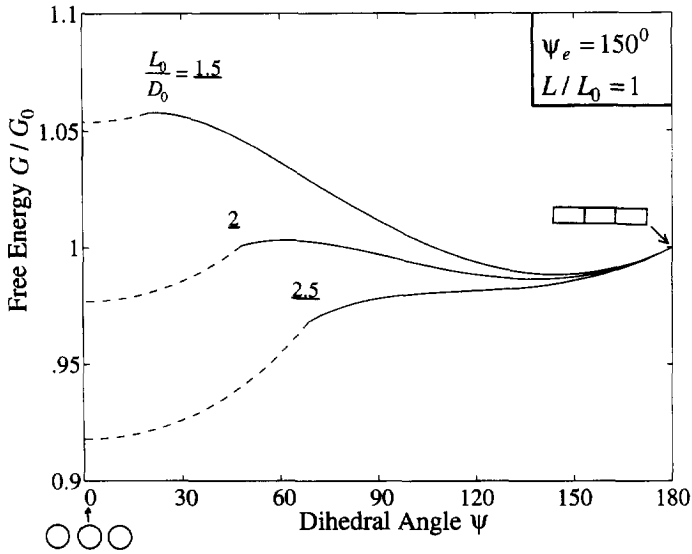

Fig. 5. Energy of a constrained fiber ($L/L_0 = 1$). The grains change shape without shrinkage before pinching off.

similar length. Grains of large diameter remained connected, but grains of small diameter broke into droplets (Fig. 1).

In this paper, we will model a situation where the fiber is unconstrained, allowing the grain length to change. Our model reproduces that of Miller and Lange in the limit $M_b/M_s \to 0$. That is, the grain-boundary mobility is so low that the grains do not change length. We will still approximate each grain by a barrel, described by two generalized coordinates: the dihedral angle Ψ and the grain length L. The free energy G, normalized by that of the initial cylindrical-shaped grain G_0, is a function of the two coordinates and the two control parameters L_0/D_0 and γ_b/γ_s

$$\frac{G}{G_0} = g\left(\frac{L}{L_0}, \Psi; \quad \frac{L_0}{D_0}, \frac{\gamma_b}{\gamma_s}\right). \tag{5}$$

The explicit function is given in Appendix A.

For a given pair of the control parameters, the energy function is a surface in the space spanned by the free energy and the two generalized coordinates. Figure 6 shows the energy landscape for $L_0/D_0 = 2.5$ and $\Psi_e = 150°$. A point on the surface represents a state, generally a nonequilibrium state. The upper left corner of the surface terminates when the grains pinch off. Indicated on the landscape are the three special states: the initial cylinders, the isolated spheres, and the truncated spheres. From the initial state of cylinders, the landscape descends steeply towards the minimum energy state of truncated spheres. The landscape, however, does contain descending paths from the state of cylinders to the state of isolated spheres.

Now compare the viscosities of the two paths. Figure 7 locates the three special states in the plane of the generalized coordinates. For the grains to approach the isolated spheres, atoms must diffuse along the surface from the triple junction to the

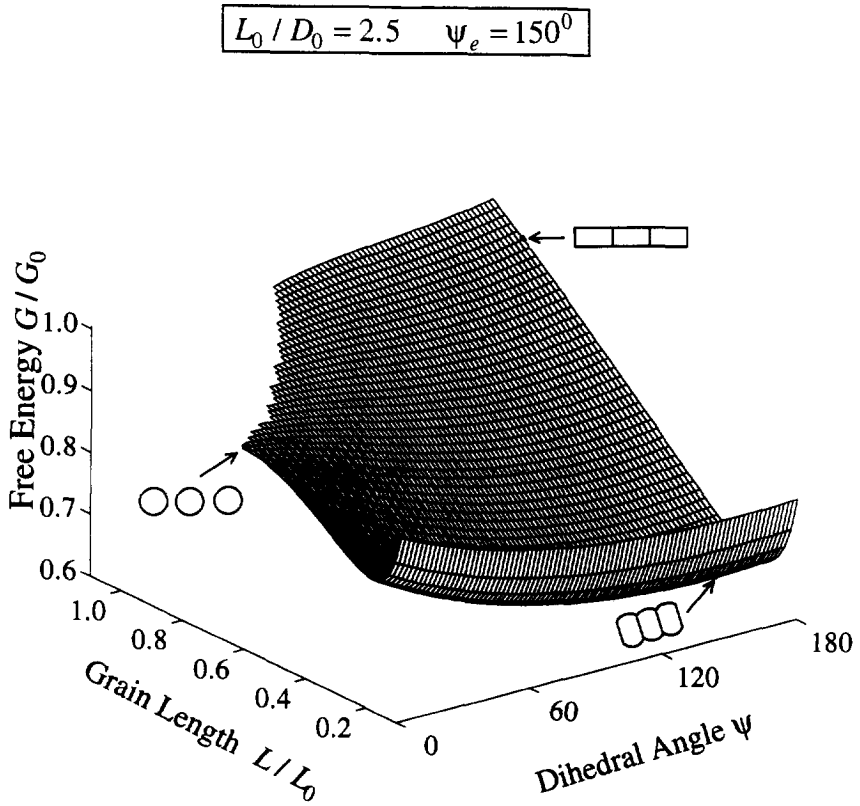

Fig. 6. Energy landscape. The free energy is a function of the generalized coordinates, represented as a surface in the thermodynamic space. A point on the surface represents a state, generally not in equilibrium. Three special states are indicated on the surface: the initial cylinders, the isolated spheres, and the truncated spheres.

middle of the free surface, the grain-boundary area decreases, and eventually the grains pinch off; the process does not require atoms to diffuse on the grain boundary. On the other hand, for the grains to approach the truncated spheres configuration, atoms must diffuse out of the grain boundaries and plate on the surface, to allow the grains to shrink. The ratio M_b/M_s is typically very low for most solids. Consequently, the path to the isolated spheres has lower viscosity than the path to the truncated spheres. The actual path results from a compromise between the energetics and the kinetics. In this description, we have loosely used the idea of viscosity on the landscape. The following section will provide a more precise description of this concept.

4. DEFINITION OF VISCOSITY MATRIX

4.1. *A virtual motion conserves mass*

The fluxes, J_s and J_b, obey certain relations required by mass conservation. They are listed as follows, with reference to Fig. 4. At a triple junction, atoms flowing out of the grain-boundary must flow onto the contacting surfaces, namely

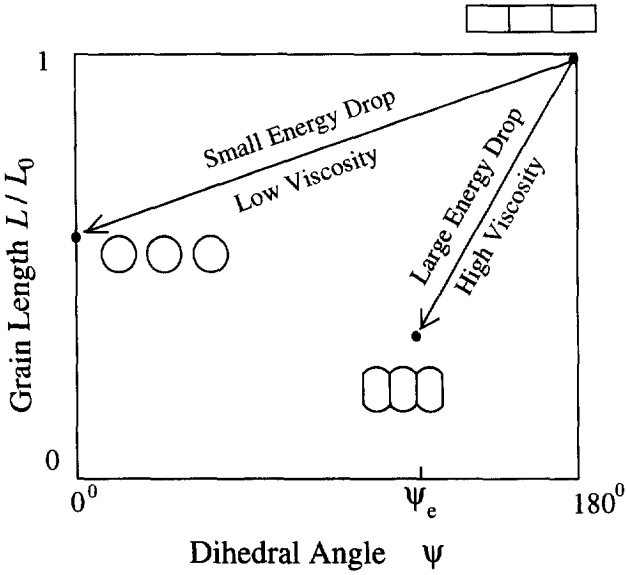

Fig. 7. Two hypothetical evolution paths, assuming a low value of M_b/M_s, drawn in the plane of the generalized coordinates. The path from the cylinders to the isolated spheres has a small energy drop and low viscosity. The path from the cylinders to the truncated spheres has a large energy drop and large viscosity. The actual path results from a compromise between the energetics and kinetics. See Fig. 8 for the calculated paths.

$$(J_b)_{tri} = (2J_s)_{tri}. \tag{6}$$

Symmetry requires that J_s vanish at the mid-point on the surface, and J_b vanish at the center of the grain boundary.

As atoms diffuse on the surface, the solid may erode or grow. Let V_s be the surface velocity (i.e. the volume of atoms added to unit area per unit time). Let (X, Y) be a point on the surface, and (n_X, n_Y) be the unit normal to the surface at this point. The surface velocity is given by

$$V_s = \dot{X}n_X + \dot{Y}n_Y. \tag{7}$$

The superimposed dot means the time derivative. Mass conservation requires that the surface velocity be balanced by the surface flux divergence

$$\frac{V_s}{\Omega} + \frac{\partial(YJ_s)}{Y\partial l} = 0, \tag{8}$$

where Ω is the atomic volume, and l the arc length.

Let V_b be the volume of mass inserted to the unit area of a grain boundary per unit time, and Y be the position of a point on the grain boundary. Mass conservation requires that

$$\frac{V_b}{\Omega} + \frac{\partial(YJ_b)}{Y\partial Y} = 0. \tag{9}$$

In the case where the two grains approach each other, we assume that no creep deformation occurs inside each grain. Consequently, V_b is constant along the grain boundary, $V_b = \dot{L}$.

There are infinitely many flux and velocity distributions that conserve mass. They are *virtual fluxes* and *virtual velocities*. A virtual motion conserves mass, but need not obey the kinetic laws (3) and (4). The *actual motion* both conserves mass and obeys the kinetic laws.

4.2. *Principle of virtual motion; variational principle*

The fluxes J_s and J_b, together with the suitable velocities, constitute a virtual motion, and $\dot{G}(J_s, J_b)$ is the associated energy rate. We define the forces, F_s and F_b, as the free energy decrease associated with an atom moving unit distance on the surface and grain boundary, respectively. Transcribing the words into an equation, we define the driving forces such that, for any virtual motion

$$\dot{G}(J_s, J_b) + \int F_s J_s \, dA + \int F_b J_b \, dA = 0. \tag{10}$$

The two integrals extend over the surface and the grain boundary, respectively. The concept of virtual motion and (10) completely define the driving forces. As shown in Appendix B, this definition is consistent with that of Herring on the basis of chemical potentials. The forces so defined drive the *actual fluxes* according to the kinetic laws (3) and (4).

Equation (10) has an alternative interpretation. The first term is the virtual energy rate, and the sum of the other two is the virtual dissipation. The equation says that, for any virtual motion, the free energy decrease balances the dissipation rate. One may call (10) the *principle of virtual motion*. Note that we exclude any dissipation term associated with the motion of the triple junction. This guarantees local equilibrium at the junction, i.e. the balance of the surface tensions (2); see Appendix B.

The principle of virtual motion, together with the kinetic laws (3) and (4), implies a variational principle. Let J_s and J_b be the *actual fluxes* that both conserve mass and obey the kinetic laws (3) and (4), and let δJ_s and δJ_b be the changes in the fluxes that conserve mass. Applying the principle of virtual power (10) to this change gives

$$\dot{G}(\delta J_s, \delta J_b) + \int \frac{J_s}{M_s} \delta J_s \, dA + \int \frac{J_b}{M_b} \delta J_b \, dA = 0. \tag{11}$$

Here the forces have been replaced by the actual fluxes according to the kinetic laws. The energy G does not depend on the fluxes, so that the energy rate is linear in the fluxes, $\dot{G}(\delta J_s, \delta J_b) = \delta \dot{G}(J_s, J_b)$. The latter means the change in the free energy rate due to the change in the fluxes. Also note that, for a small change in the flux, $J_s \delta J_s = \delta(J_s^2)/2$. Consequently, (11) can be written as

$$\delta\left(\dot{G}(J_s, J_b) + \int \frac{J_s^2}{2M_s} dA + \int \frac{J_b^2}{2M_b} dA\right) = 0 \tag{12}$$

for any small virtual change in the fluxes. That is, for the actual fluxes J_s and J_b, the quantity in the bracket does not change to first order in δJ_s and δJ_b.

Denote the quantity in the bracket by

$$\Pi(J_s, J_b) = \dot{G}(J_s, J_b) + \int \frac{J_s^2}{2M_s} dA + \int \frac{J_b^2}{2M_b} dA. \tag{13}$$

At a fixed state, Π can be calculated for any virtual motion. Different virtual motions give different values of Π. Equation (12) says that, of all virtual motions, the actual motion renders Π stationary. One may confirm that the actual motion minimizes the functional (e.g. Cocks, 1992).

4.3. *Generalized coordinates, forces, and viscosities*

We now show that the variational principle assigns a viscosity matrix to every point on the energy landscape. To avoid unessential details, we will proceed formally, leaving specifics to Appendix C. In using the variational principle, it is often impractical to search for the actual motion among *all* virtual motions. Rather, one searches among a restricted family of virtual motions, and the member of the family that minimizes Π approximates the actual motion. The larger the family, the better the approximation.

We can describe the structure with n degrees of freedom, writing $q_1, \ldots q_n$ for the generalized coordinates, and $\dot{q}_1, \ldots \dot{q}_n$ for the generalized velocities. For the row of grains, we have chosen the grain length L and the dihedral angle Ψ as the generalized coordinates. We could well have approximated the arc of the surface with many straight segments, i.e. by *finite elements*, and chosen the positions of the nodes as the generalized coordinates. Modeling the arc with finite elements would have an important advantage: the process could be automated by a computer (Pan and Cocks, 1995). In this paper, however, we will follow the main flow of concepts, and use the barrel approximation throughout as an illustration.

The free energy is a function of the coordinates, but is independent of the velocities. The function $G(q_1, q_2, q_3, \ldots)$ is a surface in the space spanned by G, $q_1, \ldots q_n$. The state of the structure is a point on the surface, and an evolution path a descending curve on the surface. The generalized forces, $f_1, \ldots f_n$, are the differential coefficients of the free energy, namely

$$f_i = -\partial G / \partial q_i. \tag{14}$$

At a given point on the energy surface, the forces are the slopes of the tangent plane contacting the surface at the point. Because the energy depends on time only through the coordinates, the energy rate is

$$\dot{G} = \sum_i \frac{\partial G}{\partial q_i} \dot{q}_i = -\sum_i f_i \dot{q}_i. \tag{15}$$

The energy rate is thus linear in the velocities.

Next we observe that the fluxes are linear in the generalized velocities

$$J_s = \sum_i N_i^s \dot{q}_i, \quad J_b = \sum_i N_i^b \dot{q}_i. \tag{16}$$

The shape functions, N_i^s and N_i^b, depend on the coordinates but not on the velocities. Appendix C calculates the shape functions on the basis of mass conservation.

Now Π at a fixed state of the structure is a function of the velocities

$$\Pi(\dot{q}_1, \ldots, \dot{q}_n) = -\sum_i f_i \dot{q}_i + \tfrac{1}{2} \sum_{i,j} H_{ij} \dot{q}_i \dot{q}_j. \tag{17}$$

The dissipation term is quadratic in the generalized velocities, and is positive-definite as required by the Second Law of Thermodynamics. The coefficients H_{ij} are given by

$$H_{ij} = \int \frac{N_i^s N_j^s}{M_s} \mathrm{d}A + \int \frac{N_i^b N_j^b}{M_b} \mathrm{d}A. \tag{18}$$

They do not depend on the generalized velocities, and form a symmetric, positive-definite matrix, which we call the viscosity matrix.

The functional Π minimizes when $\partial \Pi / \partial \dot{q}_k = 0$, leading to

$$\sum_j H_{ij} \dot{q}_j = f_i. \tag{19}$$

The significance of H as a viscosity matrix now becomes evident: H_{ij} is the resistant force in the q_i direction when the state moves at unit velocity in q_j direction. Equation (19) is a set of linear algebraic equations for the generalized velocities. Once solved, they update the generalized coordinates for a small time step. The process is repeated for many steps to evolve the structure.

At a point on the energy landscape, the force vector points to the direction of the steepest descent and, according to (19), the velocity vector points in a different direction, unless the viscosity matrix happens to be isotropic (i.e. a diagonal matrix with identical elements). Consequently, the evolution path does not usually follow the trajectory of the steepest descent. Since H is positive-definite,

$$\dot{q}_i f_i = \sum_{i,j} \dot{q}_i H_{ij} \dot{q}_j > 0. \tag{20}$$

Consequently, the combination of the Second Law of Thermodynamics and linear kinetics requires that the velocity and the force vector make an acute angle.

5. INTERPLAY OF ENERGETICS AND KINETICS

We describe the grain array with two generalized coordinates: the grain length L and the dihedral angle Ψ. The generalized forces, f_L and f_Ψ, are derived in Appendix A, and the viscosities, H_{LL}, $H_{L\Psi}$ and $H_{\Psi\Psi}$, in Appendix C. They all depend on the coordinates L and Ψ, but not on the velocities $\dot{L}$ and $\dot{\Psi}$. The velocities $\dot{L}$ and $\dot{\Psi}$ obey

$$\begin{bmatrix} H_{LL} & H_{L\Psi} \\ H_{L\Psi} & H_{\Psi\Psi} \end{bmatrix} \begin{bmatrix} \dot{L} \\ \dot{\Psi} \end{bmatrix} = \begin{bmatrix} f_L \\ f_\Psi \end{bmatrix}. \tag{21}$$

This is a set of ordinary differential equations that governs L and Ψ, which we integrate numerically for the given initial conditions.

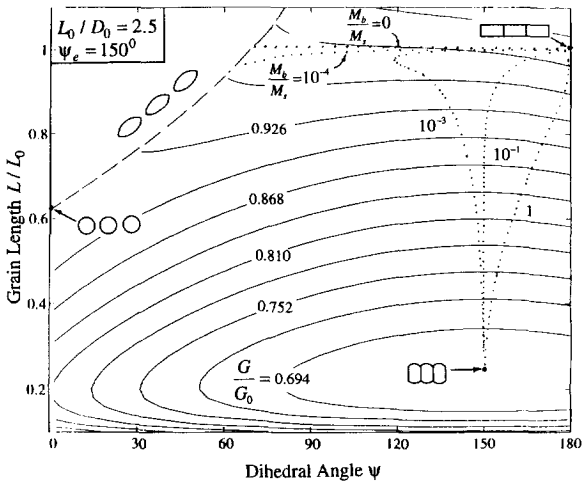

Fig. 8. The solid lines are the energy contours. The dotted lines are the evolution path when the grains are connected. The dashed line is the evolution path after the grains pinch off.

Figure 8 shows the plane of the generalized coordinates, L/L_0 and Ψ. Of the three control parameters, two are fixed at $L_0/D_0 = 2.5$ and $\Psi_e = 150°$. Indicated are the three special states: the initial cylinders, the isolated spheres, and the truncated spheres. The solid lines are the energy contours, each being the intersection of the energy landscape in Fig. 6 and a plane parallel to the coordinate-plane. One can read approximately the energy levels of the three special states. After the grains pinch off, they spheroidize with only one degree of freedom, Ψ, as represented by the dashed line at the upper left corner.

The dotted lines are the evolution paths for various mobility ratios, M_b/M_s. When the grain-boundary mobility is vanishingly small, $M_b/M_s = 0$, the grain length remains constant while the surface grooves; the grains pinch off and spheroidize, approaching a row of isolated spheres. The mobility ratio $M_b/M_s = 10^{-4}$ allows some grain shrinkage, but does not alter the destination. Increasing the mobility ratio to $M_b/M_s = 10^{-3}$ allows the grains to shrink to the state of truncated spheres. Consequently, everything else being fixed, a critical grain-boundary mobility exists, above which the grains shrink to the lowest energy state, the truncated spheres. The evolution path depends on both energetics and kinetics. Only at the mobility ratio $M_b/M_s = 10^{-1}$ does the path nearly follow the trajectory of steepest descent. Clearly this is an exception rather than a rule.

Equating the dimension in the first two terms in (9), one identifies a time scale

$$t_0 = \frac{L_0^4}{M_s \Omega^2 \gamma_s}. \tag{22}$$

Figure 9 shows plots of the grain length and the dihedral angle as functions of the normalized time. Two mobility ratios are selected, leading to different equilibrium states. Recall that, in an exact solution, the dihedral angle reaches the equilibrium value instantaneously. Within this two degrees of freedom approximation, the

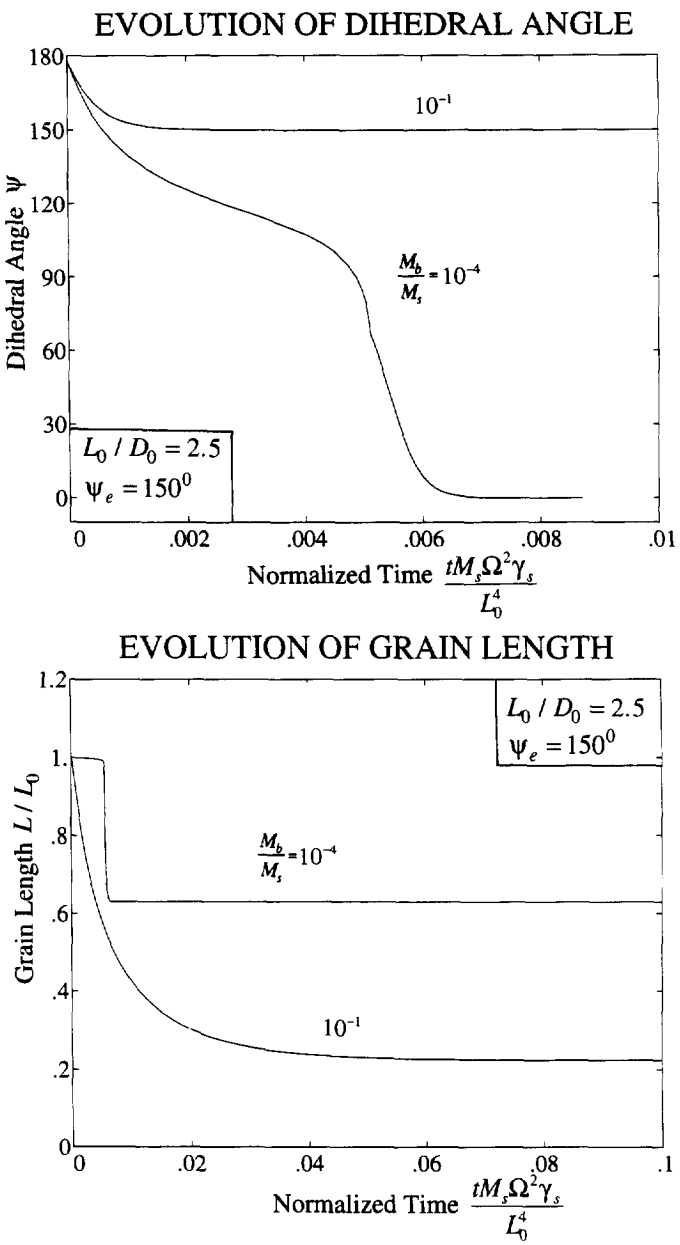

Fig. 9. Generalized coordinates as functions of time. The dihedral angle approaches its equilibrium value faster than the grain length does.

dihedral angle does not reach the equilibrium value instantaneously, but does become close to the equilibrium value at a much earlier time than the grain length.

Simulations with various values of the control parameters, L_0/D_0 and M_b/M_s, allow

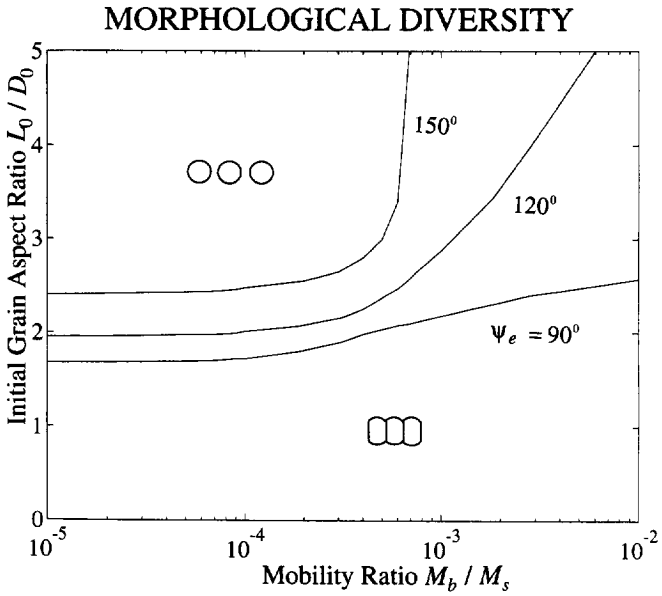

Fig. 10. Diversity map for several values of the equilibrium dihedral angles.

us to draw the diversity map in Fig. 3. Figure 10 presents the same map for several equilibrium dihedral angles. A smaller equilibrium dihedral angle corresponds to a larger grain-boundary energy, which increases the total energy of truncated spheres. As anticipated, a smaller Ψ_e moves the boundary in the map to expand the region of isolated spheres.

6. CONCLUDING REMARKS

In this paper, we have adopted a global way to look at structural evolution. One may describe an evolving structure with any kind and any number of generalized coordinates, depending on one's purpose. The free energy, as a function of the generalized coordinates, is represented by a landscape in the space spanned by the free energy and the generalized coordinates. A point on the landscape represents a (nonequilibrium) state, and the slopes of the tangent plane contacting the point represent the generalized forces. The variational principle adds another property to the landscape: a viscosity matrix at every point. A set of ordinary differential equations governs the evolution of the generalized coordinates.

Amongst the outstanding features of this approach are that: it uniformly treats all kinds of thermodynamic forces and rate processes; it readily handles surface tension anisotropy; it avoids the issue of local equilibrium, which comes out as a consequence; it can be implemented in the three dimensions. From a mathematical point of view, the approach is a Galerkin approximation of continuum structures. When a global phenomenon is of interest, the approach reduces a continuum structure to a low-dimension dynamical system. When a phenomenon of multiple length or time scales

is of interest, the approach may be implemented as the finite element method (Needleman and Rice, 1980; Cocks and Searle, 1991; Pan and Cocks, 1995) that describes a nonequilibrium structure with many degrees of freedom. Socrate and Parks (1993) devised a finite element procedure to compute the thermodynamic forces when the elastic energy is present.

ACKNOWLEDGEMENTS

The work of Sun and Suo was supported by NSF through grant MSS-9258115, by ARPA through a URI contract N-0014-92-J-1808, and by a grant from the Advanced Micro Devices under the supervision of Dr J. E. Sanchez. The work of Cocks was supported by a visiting appointment at the University of California, Santa Barbara, partly funded by ONR through contract N00014-93-1-0110.

REFERENCES

Bower, A. F. and Freund, L. B. (1995) Finite element analysis of electromigration and stress induced diffusion in deformable solids. To appear in *Materials Reliability in Microelectronics V* (ed. A. S. Oates, K. Gadepally, R. Rosenberg and W. F. Filter). Materials Research Society.

Cannon, R. M. and Carter, W. C. (1989) Interplay of sintering microstructures, driving forces, and mass transport mechanisms. *J. Am. Ceram. Soc.* **72,** 1550–1555.

Cocks, A. C. F. (1992) Interface reaction controlled creep. *Mech. Mater.* **13,** 165–174.

Cocks, A. C. F. (1994) The structure of constitutive laws for the sintering of fine grained materials. *Acta Metall. Mater.* **42,** 2197–2210.

Cocks, A. C. F. and Pan, J. (1993) Void growth ahead of a dominant crack in a material which deforms by Coble creep. *Int. J. Fracture* **60,** 249–265.

Cocks, A. C. F. and Pan, J. (1994) The influence of an interface reaction on the creep response damaged materials. *Mech. Mater.* **18,** 269.

Cocks, A. C. F. and Searle, A. A. (1991) Void growth by grain-boundary diffusion in fine grained materials. *Mech. Mater.* **12,** 279–287.

Cocks, A. C. F. and Gill, S. P. A. (1995) A variational approach in two dimensional grain growth—I. Theory. To appear.

Du, Z.-Z., McMeeking, R. M. and Cocks, A. C. F. (1995) Work in progress.

Gill, S. P. A. and Cocks, A. C. F. (1995) A variational approach in two dimensional grain growth—II. Numerical results. To appear.

Herring, C. (1951) Surface tension as a motivation for sintering. *The Physics of Powder Metallurgy*. McGraw-Hill, New York.

Kellett, B. J. and Lange, F. F. (1989) Thermodynamics of densification: I, Sintering of simple particle arrays, equilibrium configurations, pore stability, and shrinkage. *J. Am. Ceram. Soc.* **72,** 725–734.

Klinger, L. M., Glickman, E. E., Fradkov, V. E., Mullins, W. W. and Bauer, C. L. (1995) Extensions of thermal grooving for arbitrary grain-boundary flux. Submitted to *J. Appl. Phys.*

Loge, R. E. and Suo, Z. (1995) Nonequilibrium thermodynamics of ferroelectric domain evolution. Submitted to *Acta Metall. Mater.*

Miller, K. T. and Lange, F. F. (1989) The morphological stability of polycrystalline fibers. *Acta Metall.* **37,** 1343–1347.

Mullins, W. W. (1957) Theory of thermal grooving. *J. Appl. Phys.* **28,** 333–339.

McMeeking, R. M. and Kuhn, L. T. (1992) A diffusional creep law for powder compacts. *Acta Metall. Mater.* **40,** 961–969.
Needleman, A. and Rice, J. R. (1980) Plastic creep flow effects in the diffusive cavitation of grain boundaries. *Acta Metall.* **28,** 1315–1332.
Pan, J. and Cocks, A. C. F. (1993a) The effect of grain-size on the stress field ahead of a crack in a material which deforms by Coble creep. *Int. J. Fracture* **60,** 121–134.
Pan, J. and Cocks, A. C. F. (1993b) Computer simulation of superplastic deformation. *Comp. Mater. Sci.* **1,** 95–109.
Pan, J. and Cocks, A. C. F. (1995) A numerical technique for the analysis of coupled surface and grain-boundary diffusion. To appear in *Acta Metall. Mater.*
Socrate and Parks (1993) Numerical determination of the elastic driving force for directional coarsening in Ni-superalloys. *Acta Metall. Mater.* **41,** 2185.
Sofronis, P. and McMeeking, R. M. (1994) The effect of interface diffusion and slip on creep resistance of particulate composite materials. *Mech. Mater.* **18,** 55–68.
Srolovitz, D. J. and Thompson, C. V. (1986) Beading instabilities in thin film lines with bamboo microstructures. *Thin Solid Films* **139,** 133–141.
Sudre, O. and Lange, F. F. (1992) The effect of inclusions on densification : III, The desintering phenomenon. *J. Am. Ceram. Soc.* **75,** 3241–3251.
Sun, B., Suo, Z. and Evans, A. G. (1994) Emergence of crack by mass transport in elastic crystals stressed at high temperatures. *J. Mech. Phys. Solids* **42,** 1653–1677.
Suo, Z. (1994) Dislocation climb in the electron wind. *Mater. Res. Soc. Symp. Proc.* **338,** 379–390.
Suo, Z. (1995a) Wrinkling of the oxide scale on an aluminum-containing alloy at high temperatures. *J. Mech. Phys. Solids* **43,** 829–846.
Suo, Z. (1995b) *Structural Evolution in Materials, A Course.* Notes are available upon request.
Suo, Z. and Wang, W. (1994) Diffusive void bifurcation in stressed solid. *J. Appl. Phys.* **76,** 3410–3421.
Svoboda, J. and Riedel, H. (1995) New solutions describing the formulation of interparticle necks in solid-state sintering. *Acta Metall. Mater.* **43,** 1–10.
Svoboda, J. and Turek, I. (1991) On diffusion-controlled evolution of closed solid-state thermodynamic systems at constant temperature and pressure. *Phil. Mag. B* **64,** 749–759.
Wang, W. and Suo, Z. (1995) A simulation of electromigration-induced transgranular slits. *J. Appl. Phys.* Submitted.

APPENDIX A : GEOMETRY, ENERGY, AND FORCES

In this paper, we approximate the shape of every grain by a barrel, formed by a circular arc revolving about an axis (Fig. 4). The geometry is fully determined by three parameters, e.g. the grain length L, the diameter of the grain boundary D, and the dihedral angle Ψ. All other geometric quantities can be determined in terms of the above three parameters. The radius of the arc R, for example, is

$$R = \frac{L}{2\cos\left(\frac{\Psi}{2}\right)}. \tag{A.1}$$

Let (X, Y) represent a Cartesian coordinate system with the origin coincident with the grain center. The center of the circular arc which defines the barrel is at $X = 0$, $Y = -C$, where

$$C = R\sin\left(\frac{\Psi}{2}\right) - \frac{D}{2}. \tag{A.2}$$

Let θ be the angle that the normal to the arc makes with the Y-axis. A point on the arc is then given by

$$X = R\sin\theta, Y = R\cos\theta - C. \tag{A.3}$$

The volume of the barrel is

$$V = \pi L^3\left\{\frac{1}{6} + \frac{1}{4}\left(\frac{D}{L}\right)^2 - \frac{b}{4}\left[\tan\left(\frac{\Psi}{2}\right) - \frac{D}{L}\right]\right\}, \tag{A.4}$$

with

$$b = \frac{\pi - \Psi - \sin\Psi}{1+\cos\Psi} \tag{A.5}$$

and its surface area is

$$A_s(L, \Psi, D) = \frac{\pi L^2}{\cos\left(\frac{\Psi}{2}\right)}\left\{1 - \frac{1}{2}(\pi - \Psi)\left[\tan\left(\frac{\Psi}{2}\right) - \frac{D}{L}\right]\right\}. \tag{A.6}$$

The area of a grain boundary is

$$A_b = \pi D^2/4. \tag{A.7}$$

The grain conserves volume as it changes shape, so that the barrel-shaped grain evolves with two degrees of freedom, chosen to be L and Ψ. Equating the volume of the barrel to the volume of an initial cylinder, one can then express D in terms of L and Ψ

$$\frac{D}{L} = -\frac{b}{2} + \left[\frac{b^2}{4} - \frac{2}{3} + b\tan\frac{\Psi}{2} + \left(\frac{D_0}{L_0}\right)^2\left(\frac{L_0}{L}\right)^3\right]^{1/2}. \tag{A.8}$$

The free energy of a barrel, G, normalized by its value for the initial grain array, G_0, is given by

$$\frac{G}{G_0} = \left(\frac{L}{L_0}\right)^2\left(\frac{L_0}{D_0}\right)^2 \frac{\left[2 - (\pi - \Psi)\left(\tan\frac{\Psi}{2} - \frac{D}{L}\right)\right] + \left(\frac{D}{L}\right)^2\cos\frac{\Psi_e}{2}\cos\frac{\Psi}{2}}{\left(2\frac{L_0}{D_0} + \cos\frac{\Psi_e}{2}\right)\cos\frac{\Psi}{2}}. \tag{A.9}$$

Here D/L should be replaced by the expression (A.8). The free energy is a function of the generalized coordinates L/L_0 and Ψ, and also depends on the control parameters L_0/D_0 and Ψ_e.

The generalized forces associated with the two generalized coordinates, L/L_0 and Ψ, are given by taking partial differentiation of (A.9). Thus

$$f_L = -\partial G/\partial L, \quad f_\Psi = -\partial G/\partial\Psi. \tag{A.10}$$

For a truncated sphere in the equilibrium state, the configuration is fully determined by volume conservation and the equilibrium dihedral angle. The grain length is

$$\frac{L}{L_0} = \left(\frac{L_0}{D_0}\right)^{-2/3}\left[\frac{2}{3} + \tan^2\left(\frac{\Psi_e}{2}\right)\right]^{-1/3}. \tag{A.11}$$

The free energy is

$$\frac{G}{G_0}=\frac{\left[1+\frac{1}{2}\sin^2\left(\frac{\Psi_e}{2}\right)\right]\left(\frac{L_0}{D_0}\right)^{4/3}}{\cos\frac{\Psi_e}{2}\left(1+\frac{1}{2}\cos\frac{\Psi_e}{2}\right)\left[\frac{2}{3}+\tan^2\left(\frac{\Psi_e}{2}\right)\right]^{1/3}}. \tag{A.12}$$

The diameter of each isolated sphere is

$$\frac{L}{L_0}=\left(\frac{L_0}{D_0}\right)^{-2/3}\left(\frac{2}{3}\right)^{-1/3} \tag{A.13}$$

and its free energy is

$$\frac{G}{G_0}=\frac{2\left(\frac{L_0}{D_0}\right)^2\left(\frac{L}{L_0}\right)^2}{2\frac{L_0}{D_0}+\cos\frac{\Psi_e}{2}}. \tag{A.14}$$

APPENDIX B: PRINCIPLE OF VIRTUAL POWER AND HERRING'S CHEMICAL POTENTIAL

We show that the combination of mass conservation and the principle of virtual power leads to the expressions of the atomic driving forces obtained by Herring (1951). There are stresses on the grain boundary. Let σ be the stress component normal to the grain boundary. We now prescribe an arbitrary distribution of velocity, V_b on the grain boundary, V_s on the free-surface, and u at the triple junction (in the Y direction). The energy rate per grain associated with this virtual motion is

$$\dot{G}=-2\pi\int\sigma V_b Y\,\mathrm{d}Y+2\pi\int\gamma_s\kappa V_s Y\,\mathrm{d}l+\pi D\left(\gamma_b-2\gamma_s\cos\frac{\Psi}{2}\right)u. \tag{B.1}$$

The first term is the work done to insert mass on the grain boundary. The second term results from the addition of mass on the free surface, where κ is the sum of the principal curvatures of the surface. The third term is due to the motion of the triple junction in the Y direction. They are all obtained from elementary work considerations.

The velocities in (B.1) can be replaced by the fluxes according to the mass conservation equations (8) and (9). Integrating by parts we obtain

$$\dot{G}=-2\pi\int\frac{\partial(\Omega\sigma)}{\partial Y}J_b Y\,\mathrm{d}Y+2\pi\int\frac{\partial(\Omega\gamma_s\kappa)}{\partial l}J_s Y\,\mathrm{d}l+\pi D\Omega(\sigma J_b+2\gamma_s\kappa J_s)_{tri}+\pi D\left(\gamma_b-2\gamma_s\cos\frac{\Psi}{2}\right)u. \tag{B.2}$$

A comparison of (B.2) with the principle of virtual power (10)—both valid for any arbitrary virtual motion—leads to

$$F_b=\partial(\Omega\sigma)/\partial Y, \tag{B.3}$$

on a grain boundary,

$$F_s=-\partial(\Omega\gamma_s\kappa)/\partial l, \tag{B.4}$$

on a free surface,

$$-\sigma = \gamma_s \kappa, \tag{B.5}$$

at a triple junction,

$$\frac{\gamma_b}{2\gamma_s} = \cos\frac{\Psi_e}{2}, \tag{B.6}$$

at a triple junction.

Equations (B.3)–(B.6) are the local consequences of the principal of virtual power; they may be interpreted in terms of Herring's chemical potential. By definition, the chemical potential is the free energy increase associated with appending one atom to an element. From (B.1) it is evident that the chemical potential μ is

$$\mu = -\Omega\sigma, \tag{B.7}$$

on a grain boundary,

$$\mu = \Omega\gamma_s\kappa, \tag{B.8}$$

on a free surface.

Equations (B.3) and (B.4) state that the forces are the negative chemical potential gradients, and (B.5) states that the chemical potential is continuous at the triple junction. Equation (B.6) cannot be expressed in terms of the chemical potential, but comes out naturally from the principle of virtual power.

APPENDIX C: THE SHAPE FUNCTIONS

For a barrel-shaped grain, the surface velocity is computed from (7), and the surface flux is integrated according to (8), giving the shape functions

$$N_L^s = \frac{R}{\Omega Y}\left[c_1\left(\frac{R\theta}{2} + \frac{R\sin 2\theta}{4} - C\sin\theta\right) + \frac{C\theta - R\sin\theta}{2\cos\dfrac{\Psi}{2}}\right], \tag{C.1}$$

$$N_\Psi^s = -\frac{R}{2\Omega Y}\left[c_2\left(\frac{R\theta}{2} + \frac{R\sin 2\theta}{4} - C\sin\theta\right) + \frac{L}{2}\frac{\sin\dfrac{\Psi}{2}}{\cos^2\left(\dfrac{\Psi}{2}\right)}(R\sin\theta - C\theta)\right], \tag{C.2}$$

where

$$c_1 = \frac{1}{2}\left[\tan\frac{\Psi}{2} - L\frac{\partial(D/L)}{\partial L} - \frac{D}{L}\right], \quad c_2 = 2\frac{L\,\partial(D/L)}{\partial\Psi} - \frac{L}{\cos^2\left(\dfrac{\Psi}{2}\right)}. \tag{C.3}$$

In the above formulas, D/L should be replaced by expression (A.8). The grain-boundary velocity is constant, $V_b = \dot{L}$, and the shape functions for the grain-boundary flux are

$$N_L^b = -\frac{Y}{2\Omega}, \quad N_\Psi^b = 0. \tag{C.4}$$

The generalized viscosities are obtained by numerically integrating (18).